Research Article | Vol. 32, No. 16 / 29 Jul 2024 / Optics Express 28072
Optics EXPRESS

15.5 W, pulsed 630 nm generation based on Raman fiber laser and second-harmonic generation

DAL YONG LEE,[1] KYUNGSEUNG KIM,[1] CHUNGMAN LEE,[1,2] JONGWAN KIM,[3] CHANGJUN YOON,[3] JINJU KIM,[1,4] AND CHANGSU JUN[1,*]

[1]*Advanced Photonics Research Institute (APRI), Gwangju Institute of Science and Technology (GIST), Gwangju 61005, Republic of Korea*
[2]*Department of Physics and Photon Science, Gwangju Institute of Science and Technology (GIST), Gwangju 61005, Republic of Korea*
[3]*Electro-Optics Systems 2 team, Hanwha Systems, Gyeonggi-do 13524, Republic of Korea*
[4]*Currently with Korea Atomic Energy Research Institute (KAERI), Daejeon 34057, Republic of Korea*
[*]*changsu.jun@gist.ac.kr*

Abstract: We present a high-power, nanosecond 630 nm beam generation based on Raman conversion and second-harmonic generation (SHG). 116.2 W, single-mode 1080 nm fiber laser based on 10/125 μm optical fiber is used as a pump source for Raman conversion and the 1260 nm seed laser diode helps the amplification of third-order Raman conversion, which results in 63.7 W at 1260 nm with 54.8% Raman conversion efficiency. SHG to 630 nm is based on type-I noncritical phase-matching conditions with bismuth triborate (BIBO) nonlinear crystal. The average power of 630 nm is 15.5 W at a repetition rate of 9.26 MHz, a pulse width of 16.0 ns, and a SHG efficiency of 24.4%. This result can facilitate the generation of a high-power visible light source with good beam quality at a specific wavelength.

1. Introduction

The demand for high-power visible light sources is increasing for various applications including visible light communication, material processing, medical, and healthcare [1–7]. Especially, certain applications like photodynamic therapy or photo-sensitive treatment often require a specific wavelength in the visible band [4,5]. Laser diodes (LDs) or dye lasers are widely used in this wavelength region, but nearly diffraction-limited output power is usually lower than Watt-level, and further power scaling often suffers from poor beam quality [8–12]. Wavelength conversion based on solid-state laser or fiber laser can instead provide high-power visible light sources with good beam quality [13–15]. Among the visible wavelengths, high-power 532 nm and 355 nm lasers are widely found mainly due to their usage in material processing [14,16], while the power scaling in other visible wavelengths requires dedicated development [14,15,17,18]. Due to the lack of high-power, diffraction-limited blue or red light sources, the demonstration of a specific wavelength like 630 nm accompanying high-power and wavelength conversion setups is especially notable.

Second-harmonic generation (SHG) is an efficient way of generating the target visible wavelength from infrared. For that, the generation of the desired infrared wavelength is a prerequisite. However, the gain bandwidth of Ytterbium-doped lasers, despite their high output power capability, is restricted to around 1030–1120 nm [19,20]. Raman fiber laser (RFL) is a convincing alternative due to the ability to convert wavelengths to the desired range through cascaded stimulated Raman scattering. RFLs have been extensively studied with various schemes,

#532695 https://doi.org/10.1364/OE.532695
Journal © 2024 Received 13 Jun 2024; revised 13 Jul 2024; accepted 13 Jul 2024; published 18 Jul 2024

Optics EXPRESS

but a complicated setup such as Raman input/output gratings or a special component such as Raman filter fiber is sometimes required [21–23].

In this study, we present a high-power, nanosecond 630 nm light source with nearly diffraction-limited beam quality based on Raman fiber laser and second-harmonic generation. Our approach utilizes a polarization-maintaining (PM) 1080 nm fiber laser as the pump source to generate 1260 nm output through third-order Raman conversion. Optimizing the Raman fiber length, laser peak power, and pulse shape, third-order Raman wavelength could be maximized without the need for special components. Subsequently, type-I noncritical phase-matching (NCPM) SHG using a Bismuth Triborate (BIBO) crystal is employed to achieve the final 630 nm output.

Figure 1 is the estimated NCPM temperatures of LBO (Lithium Triborate) and BIBO (Bismuth Triborate) at infrared wavelengths [24,25]. Avdokhin et al. [14] demonstrated a high average power 615 nm beam based on NCPM SHG at 1230 nm with LBO crystal. The scheme, however, is difficult to be applied to the generation of 630 nm due to the very low NCPM temperature at 1260 nm although the wavelength difference is 30 nm. BIBO in this study can be an alternative for the generation of 630 nm with an NCPM temperature of around 154 °C. This demonstration can facilitate the development of high-power visible light sources with nearly diffraction-limited beam quality in other wavelengths.

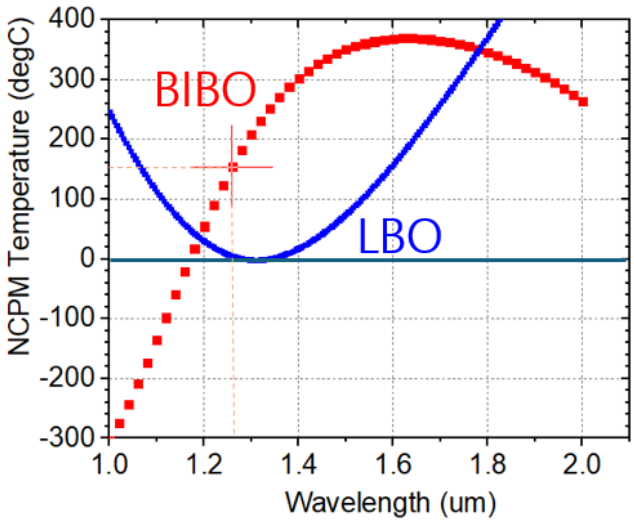

Fig. 1. Estimated NCPM temperatures of LBO and BIBO crystals at infrared wavelengths. The crossed point denotes the wavelength of 1260 nm.

2. Experimental setup

A 1080 nm Ytterbium-doped fiber (YDF) laser utilizing a three-stage master-oscillator power amplifier (MOPA) in PM all-fiber configuration serves as the pump source for the Raman amplifier. The complete setup is depicted in Fig. 2. The first row of Fig. 2 includes the 1080 nm seed laser, 1080 nm pre-amplifier, and 1260 nm Raman seed laser sections, while the second row of Fig. 2 is the 1080 nm main amplifier section. The third row of Fig. 2 is the 630 nm SHG section coupled with the fiber collimator.

The 1080 nm seed laser employs a distributed feedback (DFB) LD directly modulated by a pulsed LD driver (Aerodiode, Shaper). The seed laser beam travels through an optical isolator (ISO)/band-pass filter (BPF) hybrid component and a 99:1, 2×2 tap coupler before entering the pre-amplifier. The ISO/BPF hybrid protects the seed LD by blocking the unwanted Rayleigh

Optics EXPRESS

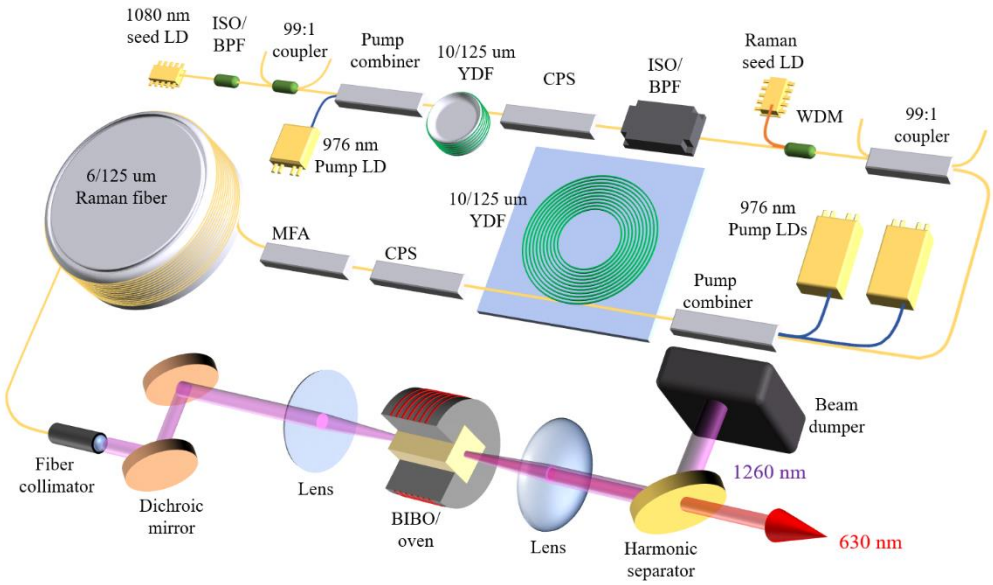

Fig. 2. Schematic diagram of the 630 nm light source. LD, laser diode; ISO, isolator; BPF, bandpass filter; YDF, Ytterbium-doped fiber; CPS, cladding power stripper; WDM, wavelength-division multiplexer; MFA, mode-filed adapter; BIBO, Bismuth Triborate.

scattering and amplified spontaneous emission (ASE) from the following pre-amplifier. The tap coupler helps monitor the forward-propagating seed LD signal and the backward-propagating pre-amplifier signal.

The 1080 nm pre-amplifier utilizes a 4.5 m-long, PM 10/125 μm YDF (cladding absorption of 4.8 dB/m at 976 nm) coiled on a small cylindrical heat sink. A pump combiner couples a 976 nm pump laser into the inner cladding of the pre-amplifier YDF. The amplified light passes through a cladding power stripper (CPS) and a high-power ISO/ BPF hybrid. The amplified pulsed 1080 nm laser and a continuous-wave (CW) 1260 nm Raman seed laser then co-propagate through a wavelength division multiplexer (WDM). The wavelength of the Raman seed laser is locked with a fiber Bragg grating (FBG) and has a 3-dB linewidth of 0.3 nm. The usage of a 1260 nm Raman seed laser with narrow linewidth helps amplify the third-order Raman signal while preventing the Raman-gain spectral broadening [26]. The 2×2 coupler after the WDM permits monitoring of the forward-propagating 1080 nm signal and the backward-propagating Rayleigh scattering, stimulated Brillouin scattering (SBS), and stimulated Raman scattering (SRS) signals from the main amplifier and Raman fiber.

In the 1080 nm main amplifier, two 976 nm pump LDs with 100 W output power each are coupled into a 4.5 meter-long, PM 10/125 μm YDF via a pump combiner. The main amplifier YDF is buried in a spiral-shaped groove structure with thermal interface material and the heat sink is water-cooled. The splicing points of both YDF ends are placed on the surface of the heat sink. After removing the residual pump power with a CPS, the signals propagate into a 40 m-long, PM 6/125 μm Raman fiber (Coherent, PM980-XP) through a mode-field adapter (MFA).

In the Raman amplifier pumped by the 1080 nm fiber laser, cascaded Raman conversion generates 1134, 1193, 1260, 1334 nm, and higher-order Raman wavelengths. To obtain the maximum power at the third-order Raman wavelength, 1260 nm seed LD was used, and the length of the Raman fiber and the peak power range of the pump laser were determined by simulation, then the peak power of the pump laser was finely optimized by tuning the repetition rate, pulse width and pulse shape of the pulsed seed laser.

Optics EXPRESS

The collimated Raman output (Beam diameter of 3.6 mm) interacts with the BIBO crystal after filtering the residual 1080 nm pump light and the low-order Raman wavelengths with the help of two dichroic mirrors. The 20 mm-long BIBO crystal is positioned in a temperature-controlled oven to satisfy type-I NCPM SHG conditions and the crystal angle, X-Y tilts can be finely adjustable to obtain maximum SHG efficiency. The frequency-doubled beam with 630 nm wavelength is separated from the fundamental wavelength of 1260 nm after being transmitted to the harmonic separator (HS).

3. Result and discussion

Figure 3(a) is the optimized result of the pulsed 1080 nm seed laser. The 3-dB linewidth of the spectrum was 1.3 nm and the 3-dB pulse width in the inset was 18.8 ns with a customized square shape. The optimized process is described in the following 1080 nm amplifier section. Figure 3(b) is the spectrum of the CW 1260 nm Raman seed laser. The 3-dB linewidth of the spectrum was 0.3 nm. The output power of the 1260 nm seed laser is approximately 500 mW.

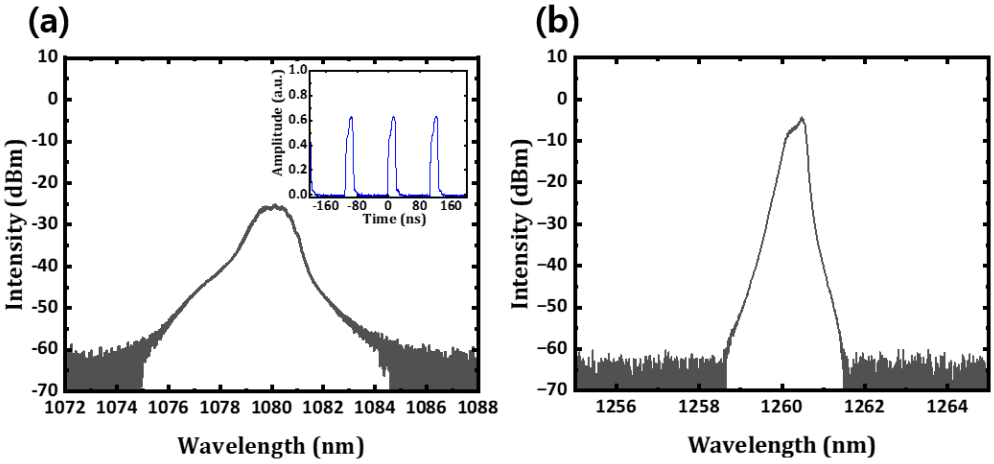

Fig. 3. (a) Spectrum and pulse train (inset) of the pulsed 1080 nm seed laser. (b) Spectrum of the CW 1260 nm Raman seed laser.

The high-power 1080 nm fiber laser was first characterized before splicing with the Raman amplifier section. The 1080 nm main amplifier was pumped by two 100 W 976 nm LDs and the PM optical fibers had the core/clad diameters of 10/125 μm. The peak power of the laser was managed to be lower than the damage threshold of the 10/125 μm silica fiber (approximately 1.5~2.3 kW) [27] and to maximize both the third-order Raman conversion and SHG efficiencies. Figure 4 depicts the output characteristics of the main amplifier. The 1080 nm output power after the CPS was 116.2 W when the 976 nm pump power was 143 W. Figure 4(a) shows the slope efficiency of 79.6%. The amplifier gain was 16.2 dB at the maximum power. The pulse energy at the maximum power was approximately 12.5 μJ when the repetition rate was 9.26 MHz. The inset of Fig. 4(a) reveals a perfectly circular Gaussian beam profile measured at the maximum output power. The measured M^2 values were 1.07 and 1.10 in x- and y-directions, respectively, confirming the single-mode operation. Figure 4(b) is the evolution of the pulse shape depending on the 1080 nm output power. The customized square pulse grows as the output power increases and the 3-dB pulse width is broadened from 19.3 ns to 20.0 ns as the 1080 nm output power is increased from 60.6 W to maximum power.

The 1080 nm laser beam was efficiently guided into the 6/125 μm Raman fiber amplifier through the MFA with a low insertion loss of 0.017 dB. As described in the experimental setup, a rough

Optics EXPRESS

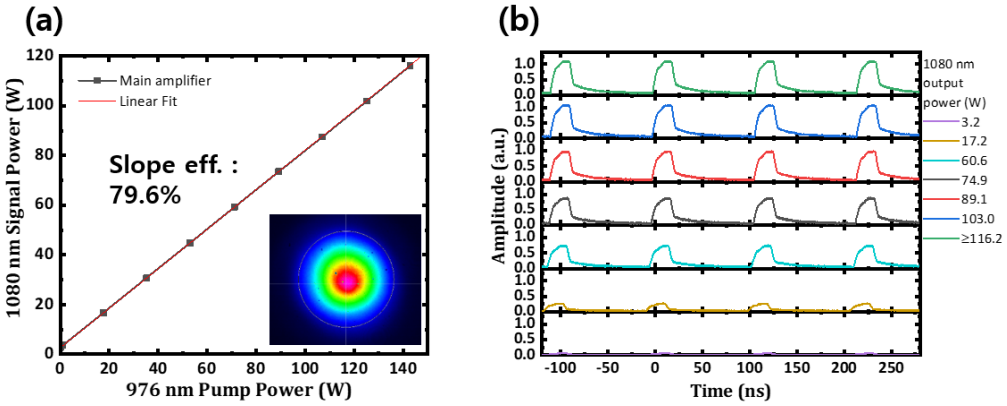

Fig. 4. Results of the 1080 nm pump laser. (a) Output power and beam profile. (b) Evolution of the pulse shape vs. 1080 nm output power.

fiber length was first determined as 40 m according to the simulation and preliminary experiment and then followed by fine-tuning of the temporal pulse characteristics and peak power to achieve maximum Raman conversion efficiency without additional filtering components. In general, high peak power is preferred for higher SHG efficiency while it can hinder specific-order (third-order) Raman conversion because of the onset of the next-order Raman wavelength. To maximize both the third-order Raman conversion and SHG efficiencies, the repetition rate was optimized in the range of 5~18 MHz, and the pulse width was optimized in the range of 5~30 ns. Additionally, several pulse shapes were compared including exponential, Gaussian, square, and customized square shapes. Among them, the customized square pulse shows the best efficiency because the wasted portion in the pulse edges which can not contribute to the nonlinear wavelength conversion can be minimized and the peaked leading edge of the pulse can be optimized by monitoring the pulse shape after amplifiers and wavelength conversion efficiencies. 1080 nm seed laser driver includes the function to adjust the level of gain-switching peak suppression of the seed LD. The tuning of the repetition rate and pulse width affects the pulse shape, resulting in the peak power variation. Therefore, fine-tuning of repetition rate and pulse width should be repeated after the pulse shape is determined. At the maximum pumping, the peak power of the 1080 nm laser entering the Raman amplifier is approximately 0.62 kW. The collimated 1260 nm RFL was characterized after filtering 1080 nm pump light and the low-order Raman wavelengths with two dichroic mirrors.

Figure 5 shows the results of the 1260 nm RFL output. 1260 nm output power is barely observed up to around 80 W of 1080 nm pump laser because first- and second-order Raman wavelengths are generated in this power range, which are filtered out. A steep increase of 1260 nm output power is observed from around 90.3 W, indicating the threshold of the third-order Raman conversion. The maximum 1260 nm output power was 63.7 W at the pump power of 116.2 W, corresponding to the third-order Raman conversion efficiency (optical-to-optical) of 54.8%. At higher pump power, the slope efficiency gradually decreases due to the generation of fourth-order Raman wavelength. The inset of Fig. 5 displays the beam profile of the 1260 nm Raman laser measured at the maximum output power. We did not have a proper beam profiler at this wavelength, but the visible to near-infrared complementary metal-oxide-semiconductor (CMOS) camera could manage to capture the beam image at high output power. It exhibits a clear Gaussian beam profile because of the single-mode nature of the 6/125 μm Raman fiber although misalignment of free-space optics in the 1260 nm monitoring setup can induce slight distortion of the beam.

Optics EXPRESS

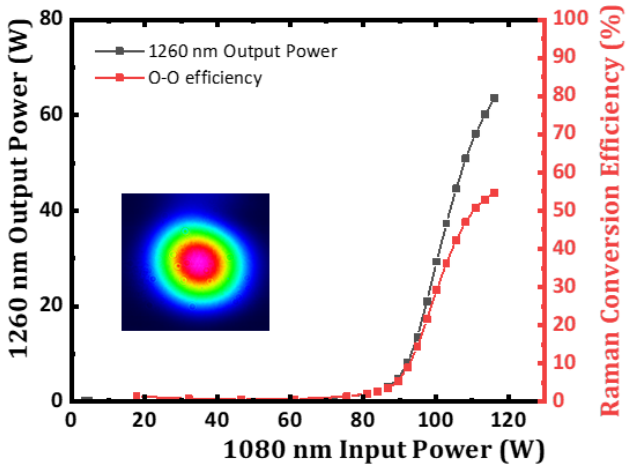

Fig. 5. Results of the 1260 nm Raman fiber laser.

Figure 6 displays the evolution of the wavelength and pulse train of the 1260 nm Raman laser depending on the 1080 nm pump power. As seen in Fig. 6(a), 1080 nm and 1260 nm signals exist when the 1080 nm pump power is 3.2 W (violet data) and the peak intensity of 1080 nm is higher than that of 1260 nm by approximately 8 dB. As the 1080 nm pump power increases, first- and second-order Raman signals are observed. At the 1080 nm pump power of 103 W (blue data), third-order Raman, 1260 nm signal has the highest intensity over the 1080 nm, 1134 nm, and 1193 nm by 13.3 dB, 12.7 dB, and 9.5 dB, respectively. At the maximum pump power (green data), the intensity of the 1260 nm signal is higher than 1080 nm, 1134 nm, and 1193 nm by 15.5 dB, 15.2 dB, and 17.0 dB, respectively. The onset of the fourth-order Raman signal with 1334 nm is observed at the maximum pump power while the intensity of it is negligible. The center wavelength of the third-order Raman signal is 1259.8 nm, and the full width at half maximum (FWHM) is 1.4 nm. In general, the Raman gain bandwidth in silica fiber is approximately 5 THz [26], but the linewidth in this experiment is maintained narrow with the help of the 1260 nm Raman seed laser. The residual pump and lower-order Raman wavelengths were negligible. Even if other wavelengths exist, they just transmit the nonlinear crystal and can be easily filtered out at the end of the SHG setup because only the 1260 nm wavelength can satisfy the SHG phase-matching conditions.

The temporal characteristics of the 1260 nm pulse are presented in Fig. 6(b). It was measured after passing two DMs which filter the residual 1080 nm pump light and the low-order Raman wavelengths. As seen in Fig. 6(b), the 1260 nm signal is not observed when the 1080 nm pump power is below 103 W (blue color), which means the inter-pulse noise is not the background or photodiode (PD) noise. From the blue and green data of Fig. 6(b), the inter-pulse noise is considered as 1260 nm and it grows as the pump power increases. In Fig. 4(b), we can see the long trailing edge in the 1080 nm output and this trailing edge seems to amplify the CW 1260 nm Raman seed output. In the SHG process, this inter-pulse 1260 nm signal will be wasted due to the low peak power, lowering the SHG efficiency. We did not analyze the percentage of inter-pulse signal this time, but reducing it by synchronously gating the 1080 nm pump laser or using an alternative driver that can enhance the modulation contrast will increase the SHG efficiency. The repetition rate of the pulse is 9.26 MHz, and the pulse width is approximately 17.9 ns and 18.7 ns when the 1080 nm pump power is 103 W and max power, respectively. The pulse energy is approximately 6.9 μJ at the maximum power and the peak power is lower than 400 W_{pp}. In general, the leading edge of the pulse is sharpened during the amplification. The

Optics EXPRESS

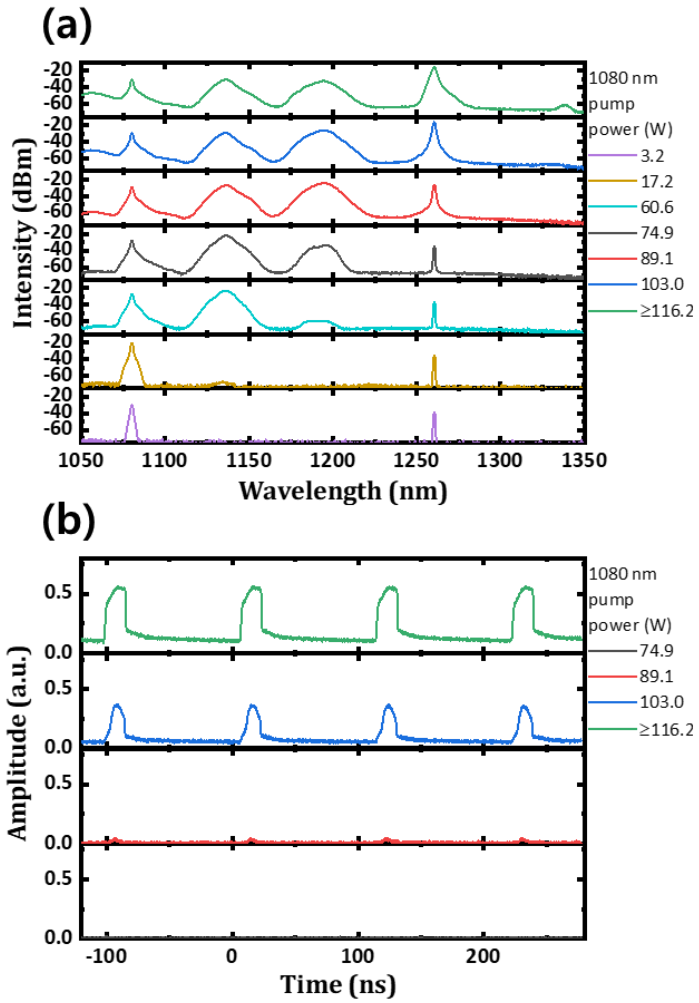

Fig. 6. Evolution of (a) the wavelength and (b) pulse shape of the 1260 nm Raman fiber laser depending on the 1080 nm pump power.

asymmetric pulse shape has an unintentionally high peak power portion, which can generate the unwanted higher-order Raman wavelength and lower the efficiency of third-order Raman conversion. Therefore, the 1080 nm seed laser pulse shape was optimized by adjusting the level of gain-switching peak suppression of the seed LD to minimize the generation of the unwanted higher-order Raman wavelengths and maximize the SHG efficiency at the maximum pumping power. The noise floor including the CW component in Fig. 6(b) is naturally filtered out at the end of the SHG setup because it cannot contribute to the frequency-doubling nonlinear process due to the low peak power.

In this experiment, germanium-doped (Ge-doped) fiber was used as a Raman fiber. Phosphosilicate (P-doped) fiber, however, as a Raman fiber can be helpful to enhance the Raman conversion efficiency because the Raman shift is three times bigger than the Ge-doped fiber, and 1260 nm can be directly generated from 1080 nm pump wavelength.

SHG for the generation of 630 nm was conducted using a BIBO nonlinear crystal. The simulation by the SNLO software [28] predicted optimal wavelength conversion under type-I

Optics EXPRESS

NCPM conditions at a crystal temperature of around 154 °C. While the simulation suggested a result of higher SHG efficiency with a 40 mm-long BIBO crystal, the crystal length in the experiment was determined to be 20 mm because it was the longest length available from the maker. The focal length of the focusing lens before the BIBO crystal was optimized in the range of 50–150 mm. The best SHG efficiency was achieved at a focal length of 75 mm. The generated 630 nm beam was separated from the fundamental wavelength 1260 nm in the harmonic separator and the residual 1260 nm was dumped.

Figure 7 displays the results of 630 nm SHG. The 630 nm output power monotonically increases up to 15.5 W when the SHG efficiency is 24.4%, while the maximum SHG efficiency of 26.7% is observed when the 630 nm output power is 13.2 W. The decrease of SHG efficiency after the maximum point is attributed to the onset of fourth-order Raman conversion in the Raman fiber although the output power of third-order Raman wavelength keeps increasing. However, the decrease of 630 nm output power after the maximum 15.5 W means that the third-order Raman wavelength begins to convert to the next order due to the increased peak power.

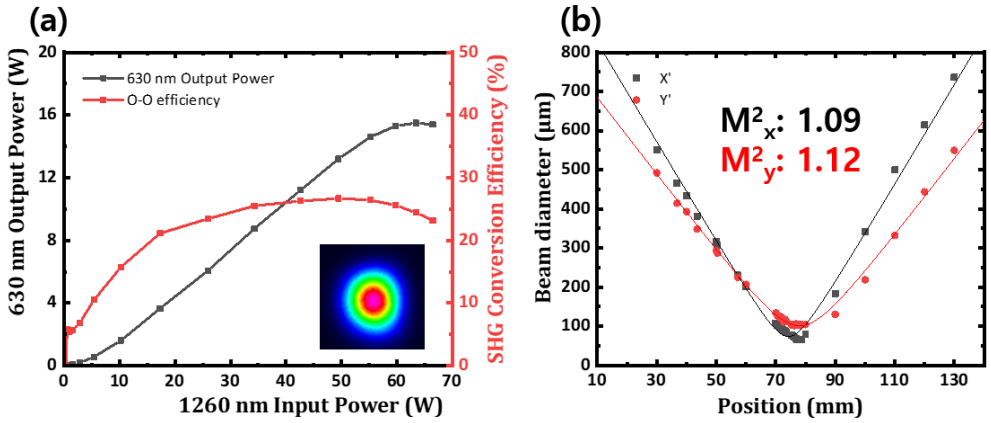

Fig. 7. Results of the 630 nm SHG. (a) Output power and conversion efficiency. (b) M^2 beam quality.

If the output power of the SHG fundamental wavelength (1260 nm) is linearly proportional to the 1080 nm pump power, then the 630 nm output power will keep increasing, unlike the saturation of Fig. 7(a). In this study, however, the saturation of 630 nm SHG output power is related to the Raman converter. As seen in Fig. 6(a), cascaded Raman conversion occurs in the Raman amplifier as the 1080 nm pump power increases. The tradeoff between the Raman amplifier and SHG restricts the 630 nm power scaling range.

The inset of Fig. 7 depicts the well-defined Gaussian beam profile of the 630 nm output. In Fig. 7(b), the measured M^2 values were 1.09 and 1.12 in x- and y-directions, respectively, confirming nearly diffraction-limited beam quality. During the SHG nonlinear process, the beam quality is enhanced because the inter-pulse CW component which is seen in Fig. 6(b) or high spatial frequency portions are compromised like the soft aperture effect [29].

Figure 8(a) is the spectrum of the 630 nm output measured at the maximum power. The center wavelength is located at 629.9 nm with a linewidth of 0.8 nm, demonstrating the characteristic spectral narrowing of nonlinear frequency-doubling.

Figure 8(b) presents the evolution of the pulse shape of the 630 nm output. The pulse period and repetition rate are identical to those of the 1260 nm Raman laser. At the 1080 nm pump power of 103 W, the pulse shape is like a triangle, which is similar with the Raman amplifier output in Fig. 6(b) because the central part which has a higher intensity than the edges contributes to the SHG process more. At the maximum pump power, the pulse shape becomes close to

Optics EXPRESS

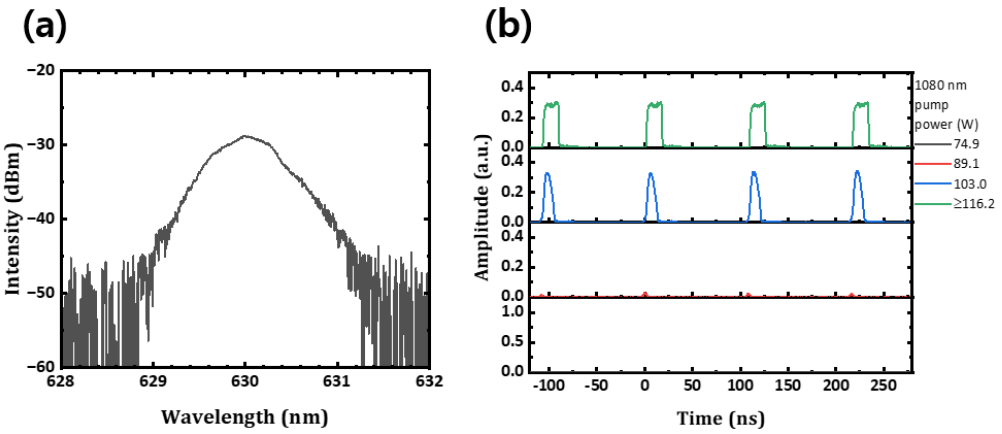

Fig. 8. Results of (a) the wavelength and (b) the evolution of the pulse shape of the 630 nm output.

square. At the maximum pump power, the pulse width of 1080 nm, 1260 nm and 630 nm output is 20.0 ns, 18.7 ns, and 16.0 ns, respectively, which becomes narrower during the nonlinear Raman conversion and SHG process. The pulse energy is approximately 1.67 μJ at the maximum power. The output powers of 1080 nm fiber laser, 1260 nm RFL, and 630 nm red laser were maintained stable without noticeable degradation during hours of experiment over several months.

4. Conclusion

We could demonstrate a stable pulsed 1080 nm fiber laser based on PM 10/125 μm with an average power of 116.2 W by managing the peak power and heat dissipation properly. Additionally, the third-order Raman conversion in a Raman fiber amplifier could be maximized with an output power of 63.7 W and a conversion efficiency of 54.8%. This was achieved without any Raman filtering components and can also be optimized in other-order Raman conversion. Integrating the high-power fiber laser and Raman fiber laser with the SHG based on BIBO nonlinear crystal, 15.5 W, nanosecond-pulsed 630 nm output with good beam quality could be successfully demonstrated for the first time. The results of the high-power Raman fiber laser can be applied to any infrared wavelength by properly choosing the seed wavelength and optimizing the Raman fiber and laser pulse parameters. Moreover, the combination of infrared Raman laser with SHG will be able to generate diffraction-limited visible light sources from blue to red wavelengths with the output power of several tens of Watts.

Funding. Defense Acquisition Program Administration (UC200013D).

Acknowledgments. This work was supported by the Defense Rapid Acquisition Technology Research Institute (DRATRI) Grant.

Disclosures. The authors declare no conflicts of interest.

Data availability. Data underlying the results presented in this paper are not publicly available at this time but may be obtained from the authors upon reasonable request.

References

1. Z. L. U. Hilan, J. I. C. Ai, Z. X. U. Engyi, *et al.*, "11.2 Gbps 100-meter free-space visible light laser communication utilizing bidirectional reservoir computing equalizer," Opt. Express **31**(26), 44315–44327 (2023).
2. K. G. Brooks and M. K. Nazeeruddin, "Laser Processing Methods for Perovskite Solar Cells and Modules," Adv. Energy Mater. **11**(29), 2101149 (2021).
3. M. Malinauskas, A. Žukauskas, S. Hasegawa, *et al.*, "Ultrafast laser processing of materials: from science to industry," Light: Sci. Appl. **5**(8), e16133 (2016).

Optics EXPRESS

4. M. Wu, X. Huang, L. Gao, *et al.*, "The application of photodynamic therapy in plastic and reconstructive surgery," Front. Chem. **10**(July), 967312 (2022).
5. W. M. Darwish, N. A. Bayoumi, H. M. El-Shershaby, *et al.*, "Targeted photoimmunotherapy based on photosensitizer-antibody conjugates for multiple myeloma treatment," J. Photochem. Photobiol., B **203**(August 2019), 111777 (2020).
6. A. V. Belikov, V. G. Kopayeva, S. Y. Kopayev, *et al.*, "Experimental and clinical study of simultaneous dual-wavelength laser action in energetic cataract surgery," Opt. Quantum Electron. **52**(3), 174 (2020).
7. S. M. Rodrigo, A. Cunha, D. H. Pozza, *et al.*, "Analysis of the Systemic Effect of Red and Infrared Laser Therapy on Wound Repair," Photomed. Laser Surg. **27**(6), 929–935 (2009).
8. N. Shimada, M. Yukawa, K. Shibata, *et al.*, "640-nm Laser Diode for Small Laser Display," High-Power Diode Laser Technol. Appl. VII **7198**, 719806 (2009).
9. S. S. Ou, J. J. Yang, R. J. Fu, *et al.*, "High-power 630-640 nm GaInP/GaAlInP laser diodes," Appl. Phys. Lett. **61**(8), 892–894 (1992).
10. Q. Yang, B. Zhang, X. Zhang, *et al.*, "A new longitudinal pumping scheme that uses elliptical laser beams to improve the compactness and efficiency of high-power dye lasers," Opt. Laser Technol. **177**(April), 111048 (2024).
11. J. A. Russell, D. P. Pacheco, H. R. Aldag, *et al.*, "Beam-quality measurements on solid state dye lasers using nonconfocal unstable resonators," in *Proc. SPIE*, R. Scheps, eds. (2001), 4267, pp. 36–45.
12. D. J. Brink and C. J. Van Der Hoeven, "Excimer-pumped dye laser with high beam quality," Rev. Sci. Instrum. **55**(12), 1948–1951 (1984).
13. H. Chi, Y. Wang, A. Davenport, *et al.*, "Demonstration of a kilowatt average power, 1 J, green laser," Opt. Lett. **45**(24), 6803 (2020).
14. A. Avdokhin, V. Gapontsev, P. Kadwani, *et al.*, "High average power quasi-CW single-mode green and UV fiber lasers," Nonlinear Freq. Gener. Convers. Mater. Devices, Appl. XIV **9347**(508), 934704 (2015).
15. P. A. Champert, S. V. Popov, A. Avdokhin, *et al.*, "Sum frequency generation of synchronously-seeded, high-power Yb and Er fiber amplifiers in periodically poled KTP," Appl. Phys. Lett. **81**(20), 3732–3734 (2002).
16. P. Ahmadi, D. Creeden, D. Aschaffenburg, *et al.*, "Generating kW laser light at 532 nm via second harmonic generation of a high power Yb-doped fiber amplifier," in *Nonlinear Frequency Generation and Conversion: Materials and Devices XIX*, P. G. Schunemann and K. L. Schepler, eds. (SPIE, 2020), 1126414, p. 40.
17. A. A. Surin, S. V. Larin, T. E. Borisenko, *et al.*, "High-power cw visible lasers pumped by Raman fibre lasers," Quantum Electron. **46**(12), 1097–1101 (2016).
18. A. M. Chandran, T. H. Runcorn, R. T. Murray, *et al.*, "620 nm Source by Second Harmonic Generation of a Phosphosilicate Raman Fiber Amplifier," in *Conference on Lasers and Electro-Optics* (OSA, 2019), paper SM3 L.4.
19. S. W. Harun, M. C. Paul, M. R. A. Moghaddam, *et al.*, "Diode-pumped 1028 nm Ytterbium-doped fiber laser with near 90% slope efficiency," Laser Phys. **20**(3), 656–660 (2010).
20. H. Zhang, H. Xiao, P. Zhou, *et al.*, "322 W single-mode Yb-doped all-fiber laser operated at 1120 nm," Appl. Phys. Express **7**(5), 052701 (2014).
21. Y. Chen, T. Yao, L. Huang, *et al.*, "2 kW high-efficiency Raman fiber amplifier based on passive fiber with dynamic analysis on beam cleanup and fluctuation," Opt. Express **28**(3), 3495 (2020).
22. V. Balaswamy, S. Arun, G. Chayran, *et al.*, "All passive architecture for high efficiency cascaded Raman conversion," Opt. Express **26**(3), 3046 (2018).
23. V. R. Supradeepa and J. W. Nicholson, "Power scaling of high-efficiency 15 μm cascaded Raman fiber lasers," Opt. Lett. **38**(14), 2538 (2013).
24. K. Kato, "Temperature-tuned 90° phase-matching properties of LiB_3O_5," IEEE J. Quantum Electron. **30**(12), 2950–2952 (1994).
25. N. Umemura, K. Miyata, and K. Kato, "New data on the optical properties of BiB_3O_6," Opt. Mater. **30**(4), 532–534 (2007).
26. G. P. Agrawal, *Nonlinear Fiber Optics*, 4th ed. (Academic, 2007), Chap. 8.
27. A. Motes and R. Berdine, "Introduction to high-power fiber lasers," Directed energy professional society (2009).
28. A. V Smith, *Crystal Nonlinear Optics: With SNLO Examples* (AS-Photonics, 2018).
29. S. Yefet and A. Pe'er, "A Review of Cavity Design for Kerr Lens Mode-Locked Solid-State Lasers," Appl. Sci. **3**(4), 694–724 (2013).